ICES Journal of
Marine Science

ICES Journal of Marine Science (2017), 74(3), 832–846. doi:10.1093/icesjms/fsw183

Original Article

Spatial distribution of the Black Sea copepod, *Calanus euxinus*, estimated using multi-frequency acoustic backscatter

Serdar Sakınan,[1,2]* and Ali Cemal Gücü[1]

[1]*Institute of Marine Sciences, Middle East Technical University, P.O. Box 28, Mersin 33731, Turkey*
[2]*Woods Hole Oceanographic Institution, Woods Hole, Massachusetts 02543, USA*

**Corresponding author: tel: +90 324 5212406; fax: +90 324 5212327; e-mail: serdar@ims.metu.edu.tr*

Sakınan, S., and Gücü, A. C. Spatial distribution of the Black Sea copepod, *Calanus euxinus*, estimated using multi-frequency acoustic backscatter. – ICES Journal of Marine Science, 74: 832–846.

Received 19 July 2015; revised 26 September 2016; accepted 28 September 2016; advance access publication 6 November 2016.

The copepod *Calanus euxinus* is a key prey species for fish in the Black Sea. To estimate the distribution and biomass of the late developmental stages of this species in July 2013, we analysed multi-frequency (38, 120, and 200 kHz) echo-sounder data from a fisheries survey of the Black Sea. The dependence of acoustic backscatter on frequency, i.e. the frequency response, was estimated for daytime scattering layers, which were confirmed by net catches to be dense, post-copepodite-stage (C4) aggregations of *C. euxinus* with prosome lengths greater than 2 mm. The high-resolution acoustic observations revealed that the nighttime, shallow distribution was bounded by the lower portion of the thermocline and that the daytime, deep distribution was bounded by oxygen. The dense and isolated aggregations were observed in seawater with a specific density, σ_T, of between 15.2 and 15.9 kg m^{-3}. These results show that fisheries acoustic surveys, typically targeting only commercially exploited fish species, may also provide information on the lower trophic levels and thereby serve as an ecosystem-monitoring tool.

Keywords: diel vertical migration, fisheries survey, frequency response, oxygen minimum zone.

Introduction

The copepod *Calanus euxinus* is one of the most common and abundant mesozooplankton species in the Black Sea and is a key component of the food web (Vinogradov *et al.*, 1992). Estimates of its abundance and spatial distribution may help explain abrupt fluctuations observed in the pelagic fish populations in the Black Sea (Ivanov *et al.*, 1998). Past studies of *C. euxinus* have investigated its vertical distribution (Vinogradov *et al.*, 1992), physiology (Svetlichny *et al.*, 2000), grazing behaviour (Besiktepe *et al.*, 1998, 2005), diapause and response to environmental conditions such as temperature and oxygen concentration (Svetlichny and Hubareva, 2005; Svetlichny *et al.*, 2006, 2009). This species congregates during the day and forms homogeneous dense layers within the oxygen minimum zone (OMZ), where individuals are safe from predation. The late copepodite stages (C4–C5) and the adults survive in the near-suboxic interface by decreasing their oxygen consumption rate (Vinogradov *et al.*, 1992). Off the Turkish Black Sea coast, in summer, Besiktepe (2001) observed a clear diel vertical migration (DVM) pattern in stratified net samples. The dense layer was sampled in the OMZ during the day and closer to the sea surface during the night.

The low spatial resolution inherent in net sampling, however, may be inadequate to characterize the patchiness of the population (Omori and Hamner, 1982). In contrast, acoustic methods may provide an effective and efficient means for estimating the biomass of patchily distributed zooplankton populations. The frequency dependence of acoustic backscatter, the frequency response, can be used to apportion echoes to target species versus other sound scatterers (Holliday *et al.*, 1989; Mitson *et al.*, 1996; McKelvey and Wilson, 2006), but the resulting classifications must be confirmed by independent measures (Foote and Stanton, 2000; Simmonds and MacLennan, 2005). Confirmation is necessary because acoustic backscatter from plankton varies with animal size; sound speed contrast, *h*; density contrast, *g*; and the

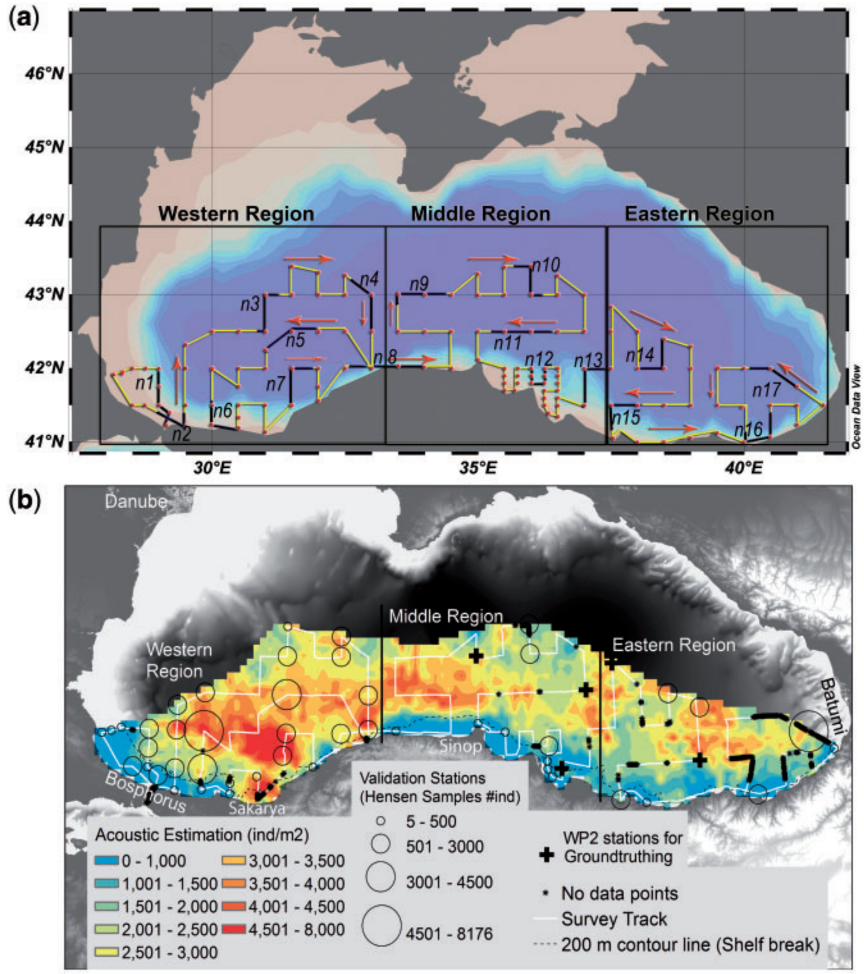

Figure 1. (a) The survey map showing the cruise track, light conditions and sampling locations. The light-colored segments on the line represent the daytime, while dark represent the nighttime (between sunset and sunrise). The numbers with the label "n" show the sequence with respect to time. Arrows represent the cruise direction. The red dots on the survey line represent the CTD stations. Large grids separate the study area into three subareas taking account of the general circulation pattern of the region. (b) Spatial distribution of the *C. euxinus* density. The gradient map shows the acoustically estimated numerical densities (ind. m-2) as interpolated with ordinary kriging. The circles show the magnitude of the densities obtained from the plankton net used for the validation. The cross symbols represent the ground-truthing stations. The white line shows the survey track and the dashed black line represent the 200 m depth contour. The dots show the no data points. The vertical lines show the sub areas. The background map represents the bathymetry from 0 to 2200 m.

incidence angle of the acoustic wave, which changes with animal orientation (Stanton *et al.*, 1996; Lavery *et al.*, 2007). At the frequencies typically used for fisheries surveys, backscatter from "fluid-like" copepods is in the Mie scattering regime, with the transition from Rayleigh-to-geometric scattering (Stanton and Chu, 2000). Furthermore, zooplankton often occur as communities of heterogeneous species composition along with larger micronekton and fishes; therefore, in many ecosystems, the backscatter from copepods can be difficult to discern or is often overwhelmed by scattering from larger organisms (Lavery *et al.*, 2007). However, in the Black Sea, *C. euxinus* is highly abundant and large, and the community of other large zooplankton is sparse.

In the Black Sea, acoustic methods are commonly used to estimate the biomasses of fish populations. In these analyses, the diffuse echoes from zooplankton aggregations have been considered noise (Stepnowski *et al.*, 1993). However, analyses of this "noise" have begun to provide estimates of the distribution and behaviour of the zooplankton populations in the Black Sea (Mutlu, 2003, 2005, 2006) and their associations with the physical properties of seawater (Mutlu, 2007).

The Black Sea is the largest anoxic basin in the world, and the water is persistently stratified due to a steep salinity gradient that limits vertical mixing (Murray *et al.*, 2006). The permanent pycnocline separates the well-oxygenated surface layer from the anoxic, hydrogen-sulphide-containing deeper water. The transition depth between these layers follows isopycnal surfaces, is dome shaped, and varies from 70 m in the centre of the basin to 200 m on the periphery due to variability in the horizontal circulation (Tebo *et al.*, 1991; Tuğrul *et al.*, 1992; Tuzhilkin 2008). Near the transition, where the specific density, σ_T, ranges from 15.2 to 15.9 kg m^{-3}, the oxygen concentration drops sharply below 1 mg l^{-1}, generally defining the OMZ (Svetlichny *et al.*, 2006). Animals in the OMZ adapt with hypoxia-tolerant vertical positioning (Vinogradov *et al.*, 1985).

To study *C. euxinus*, including its biomass, distribution, and association with the OMZ, we examined echo sounder data

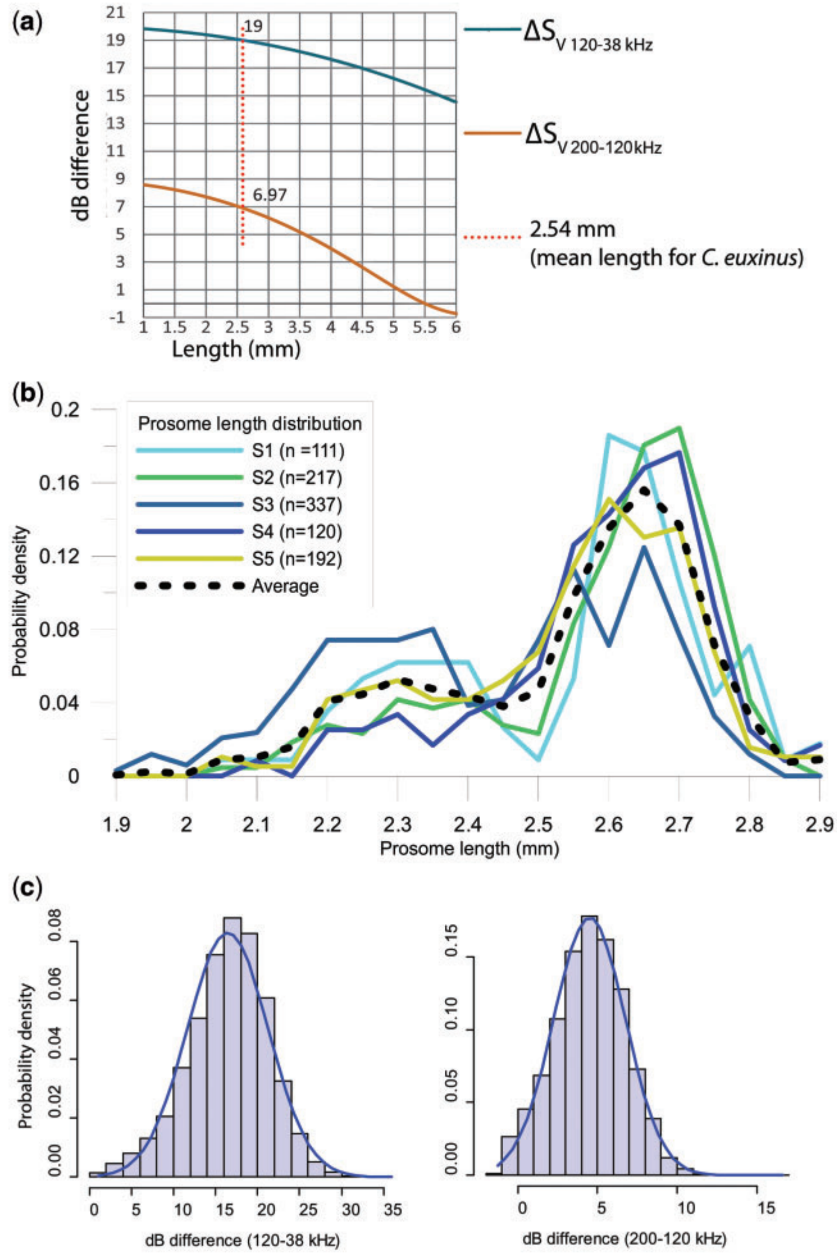

Figure 2. (a) Expected dB differences for different frequency pairs as predicted by DWBA model with respect to length interval from 1 mm to 6 mm. Dotted vertical line show the average prosome length of the observed specimens from the ground-truthing plankton net samples. (b) Length distribution measured from the samples collected at the ground-truthing stations with WP2 net. The different coloured curves show the probability density distributions from different stations, dashed line show the average. (c) Histogram of combined probability densities of ΔSV 120–38 and ΔSV 200–120 data from concentration layers of five ground-truthing stations. Layers were identified as Calanus layers by net samples. Overlaid are the normal distribution curves calculated from the observed mean and standard deviations.

collected during a fisheries survey in the Black Sea during July 2013. We identified copepod backscatter using differences in volume backscattering strength measured at multiple frequencies (Ballon *et al.*, 2011; Lezama-Ochoa *et al.*, 2011), the Z-score (De Robertis *et al.*, 2010; Ressler *et al.*, 2012), and both methods combined. We show that multi-frequency echo sounder data, collected routinely during fisheries surveys, can be used to monitor *C. euxinus* populations in the Black Sea and to examine the vertical distribution of *C euxinus* relative to environmental conditions at fine vertical resolution.

Methods

The data were collected during a July 2013 acoustic survey of the Turkish exclusive economic zone (EEZ) (172 000 km^2) in the Black Sea. Sampling was conducted at stations located every 0.5° longitude and 0.5° latitude. The transits between these stations

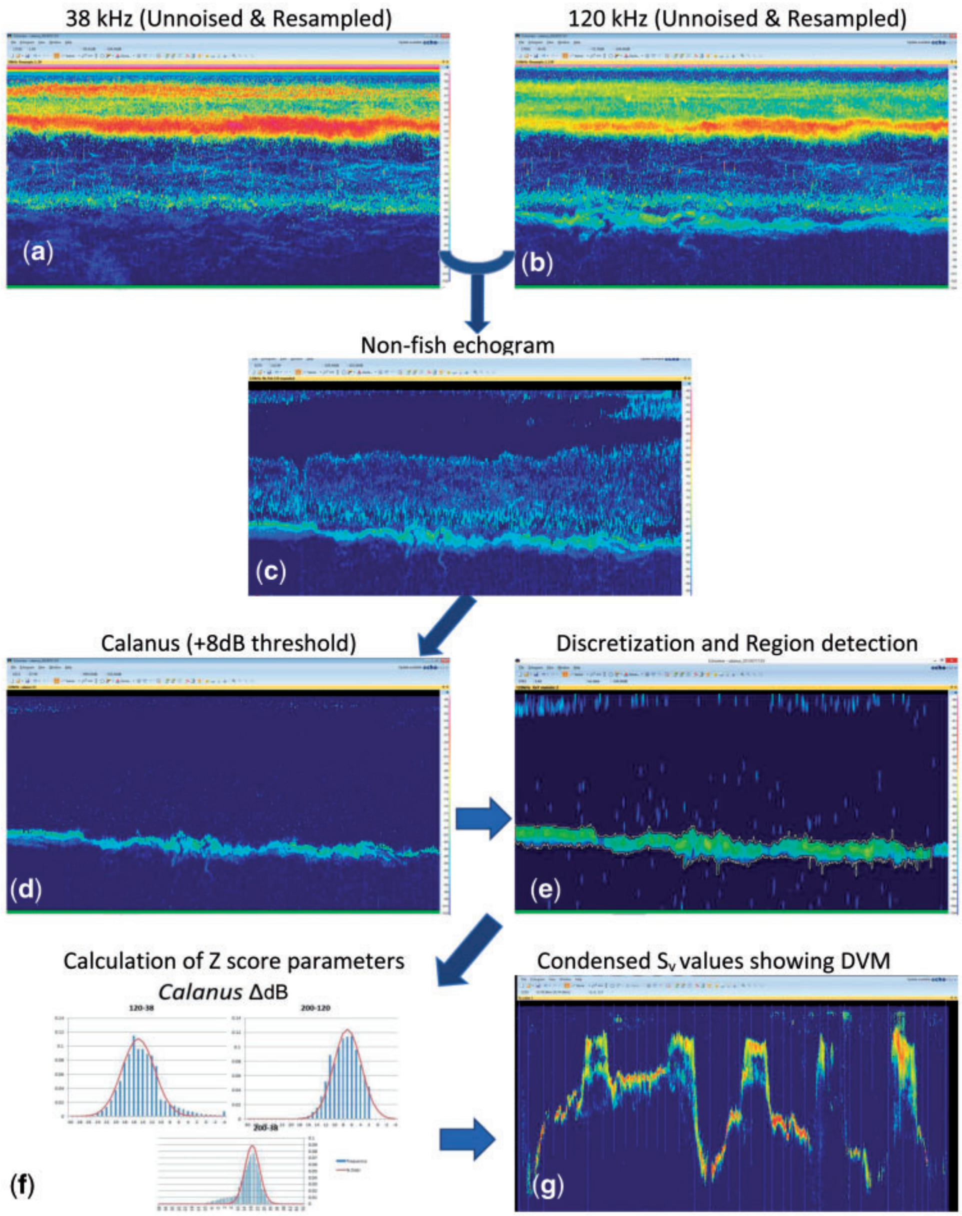

Figure 3. Processing steps used in extraction of the *Calanus* layers. (a) and (b) shows the cleaned echograms resampled into 3 pings × 0.5 m grid. (c) Shows the echogram filtered with respect to fish backscattering with +SV 120 + 38 using the method as described in Ballon *et al.* (2011). (d) Shows the potential Calanus layer as extracted using +8 dB SV 120–38. (e) Shows the discretized Calanus layer where with 3 × 3 convolution kernels and 3 × 3 erosion filter. The line encircling the boundaries of the layer was drawn by using school detection algorithm of Echoview. The +8 dB filter applied is removed after this boundary detection (f) shows example dB difference histograms where the Z-score parameters are calculated. (g) Shows the final output as pure *Calanus* backscatter. This is a condensed echogram showing the DVM pattern.

were designed to minimize the survey duration and account for wind direction. The data along the resulting track were separated into three regions (Figure 1).

Acoustic sampling

Volume backscattering strength (S_V; dB re 1 m^2) data were collected at 38, 120, and 200 kHz using an echo sounder (EK60, Simrad-Kongsberg, Norway) on RV "Bilim2" (Middle East Technical University) with split-beam transducers mounted on the hull ~4 m below the water surface. Prior to the survey, the echo sounders were calibrated with copper spheres (Foote *et al.*, 1987). The transmission power was set according to Korneliussen *et al.* (2008) to avoid nonlinear effects and cavitation. At each frequency, 0.512 ms pulses were transmitted synchronously, nominally every second (intermittently adjusted to avoid aliased seabed echoes). The vertical resolution was nominally 1/2 of the pulse length, ~38 cm. Echo data to 300 m depth (.raw format) were recorded continuously throughout the survey, day and night, along transects run at an average speed of 8 kts.

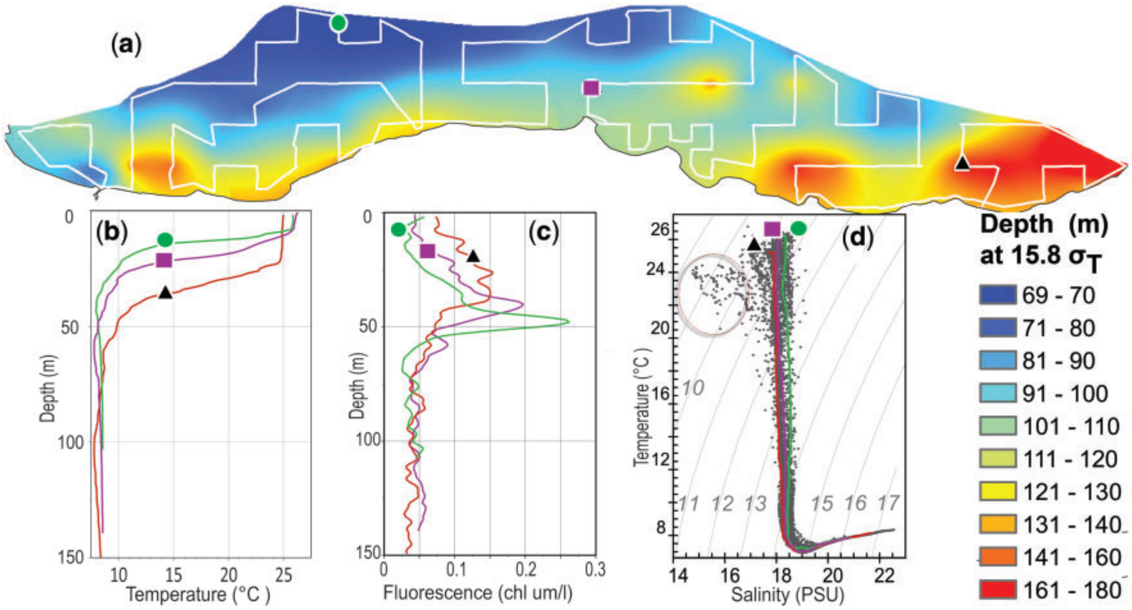

Figure 4. Environmental characteristics of the study area. (a) Shows the depth variability of the 15.8 σ_T as interpolated from the CTD measurements. The white line shows the survey track. Three marks represent different reference points with respect to circulation pattern as; the circle represent gyre centre, square represents the peripheral region and rectangle represents the eastern-anticyclonic meso-scale eddy (generally referred as Batumi gyre). (b) Shows temperature profiles at the stations marked on above map. Here, regional differences in surface mixed layer and thermocline thickness can be observed. (c) Shows the chlorophyll concentration measured as fluorescence having peaks at different depths. (d) Shows the temperature–salinity (T–S) diagram for the 135 CTD casts with the overlaid density isolines (kg m^{-3}). The encircled group of dots represents low salinity anomalies at western stations possibly due to Danube input. The values of S, T, and density are relatively above 15 σT isoline.

Hydrological and biological sampling

Conductivity, temperature, depth, and chlorophyll-a concentration were measured at each station (Figure 1a) using a CTD (SBE 9/11 plus, SeaBird Electronics, USA), and the data were processed to remove spikes. The approximate position of the OMZ was estimated from the range of σ_T=15.2–15.9 kg m^{-3}. A WP2 with a closing, 200-µm-mesh net (Wiebe and Benfield, 2003; Arashkevich *et al.*, 2014) was vertically towed to sample the scattering layers thought to represent *C. euxinus* at five stations (Figure 1b). A sensor (Simrad PI50) attached to the net provided accurate depths of the samples. Measurements of the *C. euxinus* length distribution, in 0.05-mm bins, were used to parameterize a scattering model (see "Model Predictions of Frequency Response", below) to classify echoes and estimate biomass.

In addition to conducting stratified WP2 sampling to ground truth the reference layers, catches from 45 vertical hauls with a 500-µm-mesh Hensen net (Wiebe and Benfield, 2003; Gücü *et al.*, 2016) were analysed to confirm the acoustic classifications. These hauls started at σ_T=16.2 kg m^{-3}, the lower edge of the suboxic zone, and ended at the surface. The net did not have a flow meter; thus, the areal abundance was estimated by dividing the sample density by the area of the plankton net opening. The samples were preserved with a borax-buffered 4%-formaldehyde seawater solution. In the laboratory, the samples were subsampled with a Folsom Splitter and examined under a stereo microscope. Comparisons with acoustic estimations were made using regression models separately fitted for daytime (N= 32) and for nighttime (N= 12) and using a combined model. Two nighttime samples were considered outliers and were therefore excluded from the analysis. The large discrepancy of these two samples was potentially due to the interference of dense aggregations of fish in these regions, which might have hindered acoustic detection.

Model prediction of frequency response

The Distorted Wave Born Approximation model (DWBA; Stanton and Chu, 2000, Demer and Conti, 2003) was used to predict differences in S_V from *C. euxinus* at 38, 120, and 200 kHz (i.e. $\Delta S_{V\ 120-38} = S_{V\ 120} - S_{V\ 38}$ and $\Delta S_{V\ 200-120} = S_{V\ 200} - S_{V\ 120}$) for sizes measured in samples of daytime layers (Figure 2). The DWBA includes parameters for animal shape and size; density contrast, g; sound speed contrast, h; and acoustic incidence angle (Stanton and Chu, 2000). The assumed ellipsoid shape was parameterized by measurements of the prosome length and by the dorsal and lateral width from *C. euxinus* specimens in the net samples. The seawater sound speed, $c = 1,490$ m s^{-1}, was calculated from the CTD data, and g =1.02 and h = 1.058 were taken from the literature (Lavery *et al.*, 2007). The *C. euxinus* were assumed to have a normal distribution of orientations, with their head up, on average (Thorisson, 2006), and a standard deviation (s.d.) of 30°. Based on the sampled distribution of the *C. euxinus* length, the DWBA was used to calculate a size-weighted backscattering cross-sectional area (σ_{bs}; m^2) for each frequency.

Acoustic data analysis

The acoustic data were processed using commercial software (Echoview V5.3, Sonardata, Australia) according to the following analysis procedure (illustrated in Figure 3):

(1) *Noise removal and resampling*: Noise was removed using the technique of De Robertis and Higginbottom (2007), with maximum noise threshold of −125 dB re 1 m^2 m^{-3} and a signal-to-noise ratio ≥10 dB. Noise spikes, the seabed, surface, bubble clouds, and false bottom echoes were removed using line tools (Figure 3a and b). The resulting S_V values

Table 1. Thickness of the warm surface layer and the thermocline.

		Surface layer thickness (m)			Thermocline thickness (m)		
		West	Mid	East	West	Mid	East
Off-the –shelf	Mean	17.2	15.3	17.5	7.3	20.6	16.8
	Max	21.1	18.5	29.2	4.3	4.4	6.1
	Min	11.4	10.3	10.6	13	7.5	9.6
Shelf zone	Mean	20.3	22	28.2	8.8	13.3	9.9
	Max	32.3	28.1	34.9	15.0	21.7	15.9
	Min	13.0	12.9	12.1	5.2	6.4	6.1

Mean, maximum, and minimum values are represented separately for three sub-regions and separately for shelf zone and off-the shelf zone separately. For inshore–offshore separation, 1000 m depth contour was taken as reference point. Surface layer thickness represent the depth down to temperature = 20 °C. Thermocline thickness represent thickness between temperature = 11 °C and 20 °C.

were resampled into cells of three transmissions horizontally and 0.5 m vertically.

(2) *Fish rejection*: To omit strong backscatters, e.g. fish with swim bladders, the resampled S_V values were removed if the sum of S_V measured at 38 and 120 kHz exceeded −125 dB (see details in Ballon *et al.*, 2011) (Figure 3c).

(3) *C. euxinus detection*: To identify backscatter from *C. euxinus*, the resampled S_V without fish was retained if the difference in S_V, $\Delta S_{V\ 120-38}$ ($S_{V\ 38}$ = S_V at 38 kHz, and $S_{V\ 120}$ = S_V at 120 kHz) exceeded an 8 dB threshold. This threshold was determined by modelling and corresponded to the lower bound of the dB difference possible for copepods and the upper bound of the dB difference possible for larger scatters such as fish and micronekton (Figure 3d).

(4) *Layer detection*: The S_V values ascribed to the *C. euxinus* layers were smoothed and discretized using 3 × 3 convolution and 3 × 3 erosion operators and outlined using the school detection algorithm (Figure 3e), and values of $\Delta S_{V\ 120-38}$ and $\Delta S_{V\ 200-120} = S_{V\ 200} - S_{V\ 120}$ were analysed (Figure 3f).

(5) *Z-score classification*: Data from the layers ground truthed by stratified WP2 sampling were used as a reference dataset (Supplementary Tables S2–S7) for estimating the Z-score (De Robertis *et al.*, 2010), which was calculated as

$$Z_{k,l,m} = \frac{\Delta S_{V\,v,k,l} - \mu_{k,m}}{\sigma_{k,m}},$$

where $\mu_{k,m}$ is the mean, $\sigma_{k,m}$ is the standard deviation of $\Delta S_{V\,v,k,l}$, l is the observed sample, m is the taxon, and k is the frequency pair (Figure 2). The Z-scores for each of the $n = 2$ frequency pairs were then averaged to create a confidence metric (De Robertis *et al.*, 2010):

$$\bar{Z}_{l,m} = \sum\nolimits_{k=1}^{n} |Z_{k,l,m}.$$

The resampled $S_{V\ 120}$ values without fish were filtered with a Boolean mask that retained values where $\bar{Z}_{l,m} \leq 1.6$. Due to low signal and high noise levels, respectively, the $S_{V\ 38}$ and $S_{V\ 200}$ values were not processed further.

(1) *$S_{V\ 120}$ Interpolation*: In cases where fish were present in close proximity to *C. euxinus*, gaps in the copepod-scattering layers caused by fish rejections (step 2) were filled with the average $S_{V\ 120}$ from the surrounding 0.5 n.mi. × 150-m cell. The resulting $S_{V\ 120}$ values were exported (HAC format) for further processing.

(2) *Data binning*: The exported $S_{V\ 120}$ data were binned into 10-m depths by 1-n.mi. distance cells. Cells composed of more than 95% bad data (i.e. excessive noise) were considered "no data".

(3) *Echogram resampling*: To observe the diel vertical migration pattern and compare it with hydrographic variables (Figure 3g), the binned $S_{V\ 120}$ values were resampled at 1-min intervals.

(4) *Abundance estimation*: The exported, binned $S_{V\ 120}$ data (step 7) were used to calculate the area backscattering coefficient (S_a; m^2 m^{-2}),

$$S_a = 10^{S_{V\ 120}/10} \times T,$$

where T (m) is the average cell thickness. The numerical abundance was calculated by dividing S_a in each cell by the size-weighted σ_{bs}. The diel bias observed in the numerical abundance was mitigated using the method described by Demer and Hewitt (1995). The daily-normalized abundance estimates were modelled as a Fourier series using a curve-fit algorithm (MATLAB, Mathworks, USA),

$$f(t) = a_0 + \sum_{n=1}^{h} (a_n \cos(wnt) + b_n \sin(wnt)),$$

where the w term is the sinusoidal period, t is the decimal hours, h is the number of harmonics in the series, and a_0, a_n, and b_n are the fitted coefficients. A temporal compensation function (TCF),

$$\mathrm{TCF}(t) = \frac{f(t)_{\max}}{f(t)},$$

where $f(t)_{\max}$ is the maximum value (Demer and Hewitt, 1995), was multiplied by the data.

(1) *Biomass estimation*: Bias-compensated numerical abundance values were converted to biomass using a length-versus-wet weight equation (Arashkevich *et al.*, 2014). The total biomass was estimated by (a) multiplying the biomass density by the relevant area and (b) ordinary kriging. For the latter, semi-variograms were calculated from the 1-n.mi. samples, with 1-n.mi. lag and an isotropic exponential model fit to the data without transformation. Model interpretations, trend analysis, and kriging calculations were performed using commercial software (Geostatistical Analyst, ArcMap v10, Esri, USA).

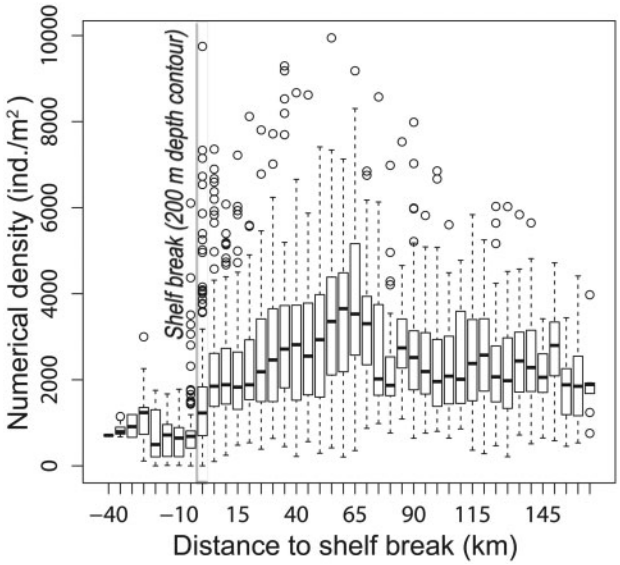

Figure 5. Box plots showing the acoustically estimated numerical density of *C. euxinus* with respect to its distance to 200 m depth contour. The middle line of each box represents the median value, the ends of the box represent the upper and lower quartiles, the whiskers represent the minimum and maximum values dots represent extreme values.

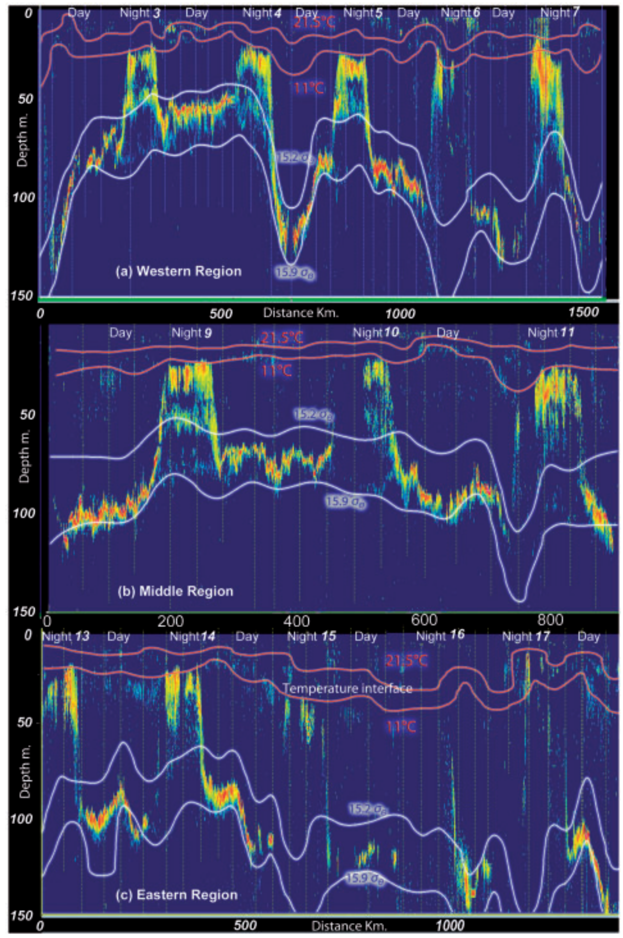

Figure 6. Diel vertical migration of C.euxinus in relation to the physical properties of the water column. (a) Western region, (b) Central region, and (c) Eastern region. Dashed vertical lines show the CTD casts. Overlaid lines represent the thermocline (upper lines 21.5 °C–11 °C) and the approximate location of the OMZ (lower lines) as represented by specific density between 15.2σT and 15.9σT. The labels on the top of the panels show the day and night sections with the sequences as shown in Figure 1.

Results

Environmental properties

The temperature and density profiles revealed the typical summer conditions of the Black Sea, with a well-developed thermocline and a warm, thin surface mixed layer (Figure 4b). The thickness of the surface layer varied considerably between the inner basin and shelf zone (Table 1). The average surface mixed layer thickness (temperature $\geq$ 20 °C) was 16 m at the inner basin (minimum, 11 m) and 24 m along the shelf (maximum, 36 m). The thermocline was between 20 and 11 °C, with an average interface thickness of 7.5 m at the inner basin (minimum, 4.4 m) and 11 m along the shelf (maximum, 21 m). The maximum temperature, 26.2 °C, was observed in the middle region, and the minimum of 8 °C occurred at 87 m in the western region. Irregularities in the temperature-salinity diagram (Figure 4d) were related to the westernmost stations, which were in low salinity water due to freshwater output from the Danube River. Apart from the local effects of the Bosphorus and Danube, the temperature-salinity values were spatially homogeneous with well-defined stratification. The thickness of the oxygenated layer varied 2.6-fold regionally due to cyclonic and anti-cyclonic large-scale eddies (Figure 4a). The σ_T= 15.8 kg m^{-3} depth, an indicator of the depth of the transition between the surface oxygenated layer and anoxia, varied inshore versus offshore and east to west (Figure 4a). This depth was a maximum of 178 m in the eastern region, also known as the Batumi anticyclonic gyre zone, and was a minimum of 63 m in central offshore waters (Figure 4a), where the large cyclonic gyres drive the circulation (Staneva *et al.*, 2001). The maximum chlorophyll-a concentration, measured as *in situ* fluorescence, was observed below the thermocline. A secondary, deeper chlorophyll-a peak was observed at the centre of each of the cyclonic regions, corresponding to the hypoxic–anoxic transition (Figure 4c) and the minimum depth of σ_T= 15.8 kg m^{-3}, as shallow as 63 m. An oxygen-density relationship (see Supplementary Data) allowed isopycnals to be used as a proxy for the low dissolved oxygen zone.

Spatial distribution

The acoustic data ascribed to *C. euxinus* comprised 81% of the 2728 1-n.mi. cells (150–1500 transmissions per cell, average = 464, s.d.=406). The remaining 19% of the cells yielded zeros. Of these zeros, 74% were in areas with a seabed depth of less than 100 m. Apart from the zeros, 9% of the cells were "no data" regions and discarded (Figure 1b). Of these excluded cells, 64% were located in the eastern region, particularly within the Batumi anticyclonic gyre, where the oxygenated depth extends below 150 m (Figure 4).

The *C. euxinus* backscattering was patchy, with the highest concentrations occurring in the western region, particularly just offshore of the shelf, where the densities reached 13 000 ind. m^{-2} (Figure 1b). This region is associated with the Rim Current,

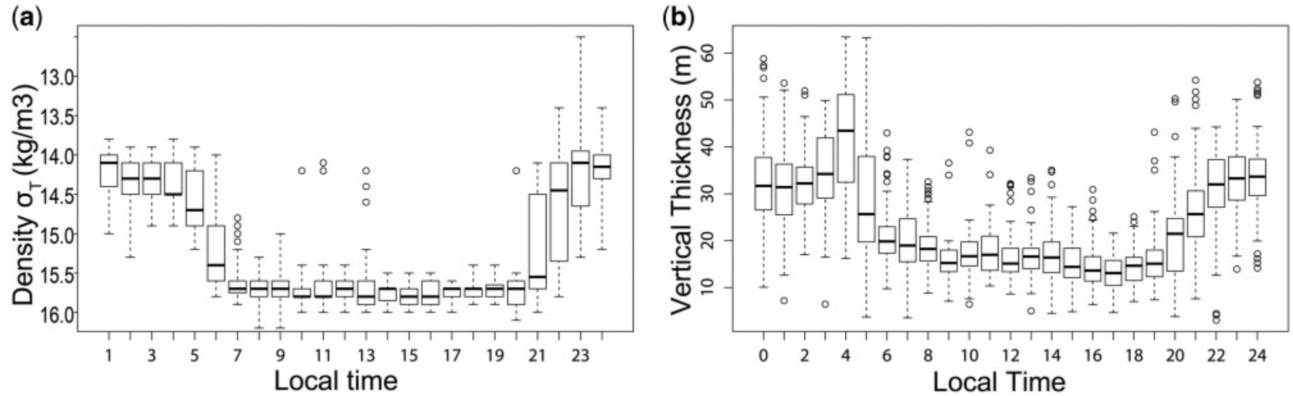

Figure 7. Diel vertical migration pattern with respect to (a) seawater density (notice daytime distribution is centred at 15.7 σ_T–15.8 σ_T levels) and (b) Average of the maximum vertical thickness of the layer of occurrence. Thickness is substantially reduced at daytime.

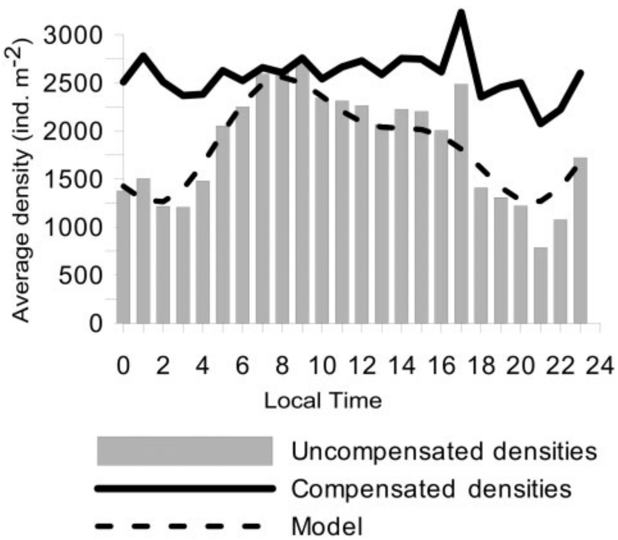

Figure 8. Daily average Calanus densities proportioned by hour of local time. Overlaid dashed line show the Fourier model fit. Black line shows the densities as compensated by the model.

which follows the shelf slope throughout the basin. A general trend was observed in the cross-shelf direction, where the abundance increased near the shelf edge and the shelf break (see 200 m depth contour in Figure 1b). Beyond this point, the abundance increased in an offshore direction to a maximum near 60 km, decreasing thereafter (Figure 5). The overall average numerical density, calculated from the acoustic backscatter, was 2241 ind. m^{-2} (CV = 76%). This value was 2741 ind. m^{-2} (CV = 55%) in the offshore zones, beyond the shelf-break. The offshore average densities were 3127 ind. m^{-2} (CV = 48%) for the western region, 2481 ind. m^{-2} (CV = 57%) for the middle region, and 2434 ind. m^{-2} (CV = 65%) for the eastern region.

Vertical distribution

The *C. euxinus* echograms revealed a clear diel vertical migration (DVM) cycle throughout most of the surveyed area (Figure 6). The vertical thickness of the *C. euxinus* layers varied throughout the day, expanding at night to a maximum average value of 40.5 m (CV = 24%) at approximately 05:00 local time (GMT + 3) and concentrating deeper during the day into a narrower layer with an average value of 12.3 m (CV = 49%) at 1600 local time (Table 1, Figures 6 and 7). The Fourier series fitted to the data (r^2 = 0.78) revealed a 24-h periodicity with a maximum in the morning, at 07:30–08:30 local time, and a secondary peak after midnight, at 01:00–02:00 local time. The maximum $f(t)$ was 2560 ind. m^{-2}, observed at 08:00 local time (Figure 8). During the night, the upper bound of the aggregations was confined by the lower boundary of the thermocline (Figure 6). During the daytime, *C. euxinus* were mostly between σ_T = 15.2–15.9 kg m^{-3} (Figures 6 and 7), corresponding to low oxygen conditions. Within this range, the intensity was not homogeneously distributed. The densest concentrations generally occurred between σ_T = 15.7 and 15.8 kg m^{-3} (Figure 7).

The diel periods were classified as daytime, upward migration, nighttime, and downward migration. The nighttime and downward migration samples were not significantly different in terms of abundance (p = 0.16). However, the upward-migration and daytime samples differed significantly (p < 0.0001), suggesting the upward-migration samples were biased from the filtering of echoes from large targets, e.g. foraging fish. This bias may also be due to changes in copepod orientation and the associated changes in incidence angle, σ_{BS}, and thus $S_{V\ 120}$ versus time.

The upward movement of the *C. euxinus* layers began at approximately 1945 local time, and the migration completed 1 h 50 min later. At the end of the vertical migration, their total backscattering values stabilized, and their density was, on average, 27% less than the daytime values (Figure 8). The downward migration began at approximately 05:25 local time and slowed near the OMZ, 45 min later. Thus, the downward migration was 1 h faster than the upward migration. Additionally, the downward movement was generally more detectable than the upward migration. In the survey region, the angle between the sun and the horizon was 18°, and the approximate times of dawn, sunrise, sunset and dusk were 04:20, 05:16, 20:18, and 22:03 local time, respectively.

Net samples

The *C. euxinus* layers were acoustically detected at depths ranging from 69 to 125 m. Their acoustically estimated numerical densities ranged from 153 to 502 ind. m^{-3}. The WP2 net samples indicated areal densities of 3790 ind. m^{-2} to 5360 ind. m^{-2}, with

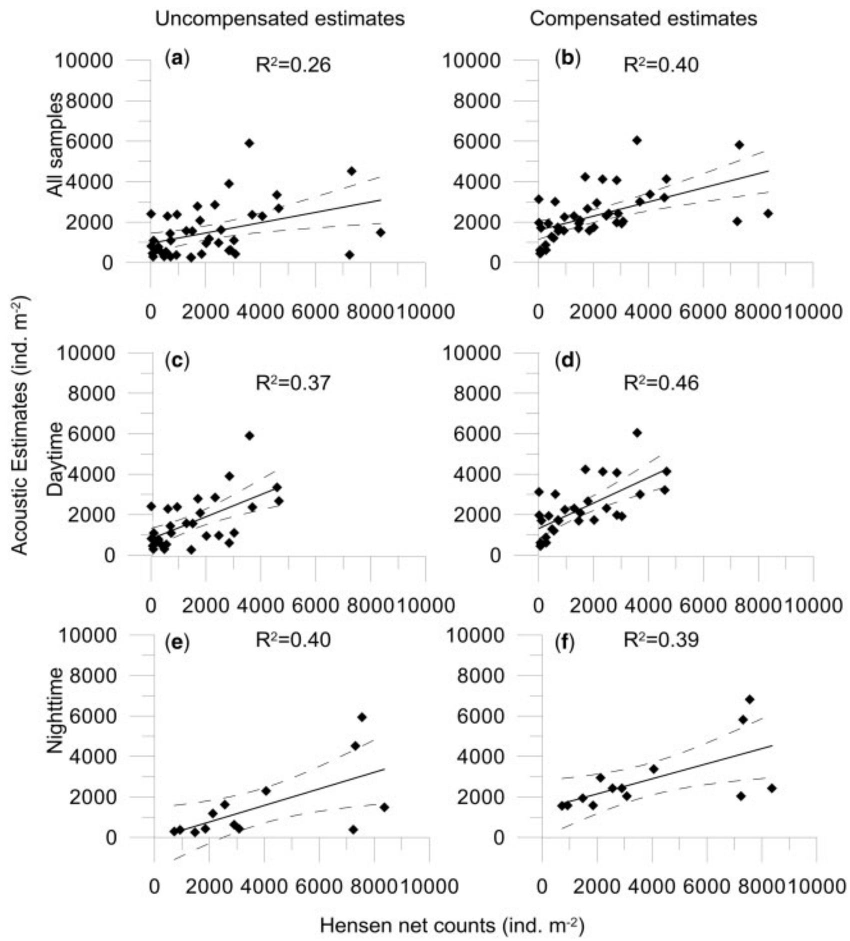

Figure 9. Scatterplots for comparison of acoustic density estimates with the Hensen net catches. Acoustic estimates represent the density calculated from extracted *Calanus* backscatter of 1 nmi sampling grid that correspond to the specific Hensen-net station. Comparisons were made for (a) whole dataset combined, (c) only daytime, (e) only nighttime. The panels (b), (d), and (f) show the comparisons made with the *f(t)* compensation (Figure 8) with respect to diel oscillations in the data. The black lines show the regression model and dashed lines show 95% confidence intervals.

an average of 4413 ind. m^{-2} (Supplementary Tables S2–S7). Specimens were 57% adult female, 33% C5 (copepodite stage), and 7% male. The prosome length distribution had modes at 2.3 and 2.65 mm (Figure 2b). The average prosome width was 0.78 mm.

Other copepods in the samples—*Pseudocalanus elongatus*, *Oithona similis*, *Paracalanus parvus*, and *Acartia clausi*—had prosome lengths $\leq$1 mm, and they therefore contributed negligible backscatter at 120 kHz (wavelength ~12.3 mm). Although the chaetognath *Sagitta setosa* was also present in the samples, average length = 15.3 mm, it had a 94% lower numerical density than *C. euxinus*.

Validation

The *C. euxinus* counts obtained from the Hensen egg nets (only copepodite stages >C4) were compared with concurrent, acoustically estimated abundances (Table 2 and Figure 9). *Sagitta setosa* was present in higher numbers in these samples than in the WP2 sample, possibly due to juveniles in the upper layers. However, the ratio of *S. setosa* adults >10 mm was still relatively low (6%) compared to the abundance of large *C. euxinus* (see Supplementary Table S7 for detailed composition). For the presence of other species, see Supplementary Table S8.

The acoustic estimates of *C. euxinus* abundance were slightly higher than the net estimates (13%). Due to the presence of two outliers, a paired t-test did not reject the null hypothesis that these populations were different ($p = 0.36$). Omitting the outliers, there was no significant difference ($p = 0.0008$). One outlier was located at the easternmost end of the study area with 8176 ind./sample. The acoustic estimate for that point was only 2413 ind. m^{-2} (Figure 1b). The sample was located within the Batumi anticyclonic gyre, where a detection problem resulted from the increased depth range of the oxygenated layer (Figure 4). Apart from this observation, the regression models showed that all comparisons were significant ($p < 0.0001$). The correlations (Figure 9) were $r^2 = 0.26$ (combined), $r^2 = 0.37$ (daytime), and $r^2 = 0.42$ (nighttime). Even after applying temporal compensation, the correlations did not differ substantially: $r^2 = 0.40$, $r^2 = 0.46$, and $r^2 = 0.39$ for the combined, daytime and nighttime estimates respectively. Regarding *S. setosa*, the relationship between juvenile abundance and the acoustic density attributed to *C. euxinus* was not significant for the 0–5 mm ($p = 0.59$) and 5–10 mm ($p = 98$) length classes. However, there was a weak but significant

Table 2. *C. euxinus* abundance estimates used in validation.

Station No	Hensen net (ind/m^2)	Lat	Lon	Time (h/GMT)	Acoustic # (ind/m^2)	Compensated Acoustic # (ind/m^2)	Date (July 2013)	Phase
2	4661	41.8	29.0	2.6	2678	4132	12	Day
3	3032	42.0	29.0	5.2	1100	1920	13	Day
6	68	42.0	28.3	8.4	779	615	13	Day
7	276	41.9	28.1	8.4	779	615	13	Day
11	18	41.2	29.5	4.4	814	1966	14	Day
12	3695	41.5	29.5	5.7	2368	3004	14	Day
13	2853	42.0	29.5	10.2	3902	4073	14	Day
14	2021	42.3	29.5	13.6	950	1736	14	Day
19	1789	43.0	31.5	5.8	2079	2660	15	Day
20	953	43.4	31.5	8.9	2376	2251	15	Day
26	2474	42.5	33.0	3.7	973	2315	16	Day
27	3589	42.0	33.0	6.9	5903	6047	16	Day
38	484	41.2	30.5	4.8	296	1285	18	Day
39	705	41.3	30.5	6.4	1434	1739	18	Day
42	1295	41.1	31.0	12.5	1567	2305	18	Day
44	1705	42.0	31.5	2.4	2784	4235	18	Day
47	263	41.6	32.0	10.3	682	873	19	Day
49	363	42.0	33.5	2.0	534	1939	19	Day
63	1463	43.0	36.0	2.9	261	1691	21	Day
72	66	42.1	35.0	9.6	454	444	23	Day
73	558	42.0	35.5	12.1	532	1207	24	Day
91	2847	41.7	36.2	1.7	602	1979	24	Day
92	732	41.6	36.2	11.8	1088	1708	25	Day
93	100	41.5	36.3	11.8	1088	1708	25	Day
94	13	41.4	36.3	15.5	2407	3127	25	Day
106	2337	42.4	38.5	4.0	2853	4127	27	Day
107	4589	42.3	39.0	8.1	3346	3213	27	Day
113	1516	41.1	37.5	5.9	1562	2093	28	Day
114	87	41.0	38.0	10.6	290	571	28	Day
123	611	41.5	41.5	15.5	2288	3007	29	Day
0	7242	41.4	29.2	22.1	385	2038	12	night
1	929	41.5	29.0	0.4	367	1579	12	night
9	1474	41.5	28.7	19.5	247	1937	13	night
15	2563	42.5	30.0	16.6	1614	2430	14	night
23	4063	43.0	32.5	17.7	2290	3375	15	night
24	2126	43.3	32.5	19.9	1177	2952	15	night
30	8368	42.5	31.5	24.0	1483	2422	16	night
36	7558	41.5	30.0	16.8	5946	6817	17	night
37	721	41.2	30.0	0.9	292	1554	17	night
43	7316	41.5	31.5	23.2	4523	5816	18	night
48	2900	42.0	32.5	20.0	626	2427	19	night
62	1853	43.4	36.0	23.4	426	1573	21	night
118	3084	41.0	40.0	22.3	422	2039	28	night

Following information are represented; station number, net estimations, location, time, acoustic estimations, compensated acoustic estimations, and the light condition.

($p = 0.01$) correlation for the adults: 10–15 mm ($r^2 = 0.127$) and 15–20 mm ($r^2 = 0.123$).

Frequency response and Z-score parameters

The results of the DWBA model were generated for *C. euxinus* lengths from 1 to 6 mm (Figure 2). For the average length of 2.54 mm, the expected $\Delta S_{V\ 120-38}$=19 dB, and $\Delta S_{V\ 200-120}$=6.97 dB. For backscatter from the net-confirmed *C. euxinus* layers, the observed distributions of $\Delta S_{V\ 120-38}$ and $\Delta S_{V\ 200-120}$ were normally distributed, with modal values ranging from 15.5 to 19.0 dB (mean = 16.8 dB and s.d.: ~1.4) (Figure 2a) and 3.9 to 5.5 dB (mean = 4.5 and s.d.= 0.6) (Figure 2a), respectively. The *Z*-score parameters, obtained through bootstrapping combination, were $\Delta S_{V\ 120-38}$=N (16.5, 4.5 dB) and $\Delta S_{V\ 200-120}$=N (4.5, 2.3 dB). For the daytime layers, C. *euxinus* *Z*-scores ($\bar{Z}_{calanus}$) between 0.75 and 0.85 (s.d.= 0.35–0.4) indicated high classification reliability. For the nighttime layers, however, $\bar{Z}_{calanus}$ was ~1.2, with a similar s.d. A value of $\bar{Z}_{calanus} \leq 1.6$ was used to identify C. *euxinus*.

Biomass estimation and potential error

The average TS, weighted by the length distribution (Table 3), was −113.3 (dB re 1 m^{-2}) for a mean weight of 1.27 mg ind^{-1}. For an average density of 2241 ind. m^{-2}, the estimated total wet

Table 3. Estimated TS and body weight.

Length	Probability density (%)	TS	Weight
1.9	0.0	−120.7	0.49
1.95	0.2	−120.0	0.53
2	0.1	−119.4	0.58
2.05	0.9	−118.8	0.63
2.1	0.9	−118.2	0.68
2.15	1.3	−117.6	0.74
2.2	4.0	−117.1	0.79
2.25	4.4	−116.5	0.85
2.3	5.2	−116.0	0.91
2.35	4.5	−115.4	0.98
2.4	4.3	−114.9	1.05
2.45	4.2	−114.4	1.12
2.5	5.2	−114.0	1.19
2.55	10.3	−113.5	1.27
2.6	13.9	−113.0	1.34
2.65	15.1	−112.6	1.43
2.7	13.9	−112.1	1.51
2.75	7.2	−111.7	1.6
2.8	2.9	−111.3	1.69
2.85	0.8	−110.8	1.79
2.9	1.0	−110.4	1.89
Scaled TS − 113.3 (dB re 1 m^{-2})			
Scaled Weight 1.27 mg			
Scaled Length 2.54 mm			

Values are scaled with respect to probability densities of length classes.

weight biomass of *C. euxinus* in the surveyed area was 490 000 tons (± 15 500 95% CI). Estimated using ordinary kriging, the mean biomass was 550 000 tons. The exponential model used in kriging produced a sufficiently good fit for the spatial variability (cross-validation slope = 0.72 and $r^2 = 0.65$). To assess potential uncertainty in *TS* due to parameterization, the *g* in the model was increased from 1.02 to the average density of 1.06 as reported in Svetlichny *et al.* (2009). As a result, the weighted *TS* increased to −108.8 (dB re 1 m^{-2}), which resulted in a 55% reduction in the total estimated biomass. To further constrain uncertainty, the assumed average prosome length was changed from 2.1 to 2.7 mm, resulting in a reduction of 45.6% in biomass and 75.4% in abundance.

The effect of environmental conditions on the *Calanus* distribution

Among the 137 CTD casts presented above, only 109 achieved a maximum depth sufficient to measure the density magnitude of $\sigma_T = 15.8$ kg m^{-3} and therefore to sample the full habitat of the *C. euxinus*. Of these 109 casts, only 96 casts coincided with acoustic detection of the *C. euxinus* layer. Among these detections, 56 casts overlapped with the daytime occurrence and 32 CTD casts with nighttime. The depth of $\sigma_T = 15.8$ kg m^{-3} was linearly correlated with the average acoustically detected daytime *C. euxinus* depth ($r^2 = 0.91$, $p < 0.0001$) (Figure 7a). In contrast, the lower thermocline depth (corresponding to 11 °C) was significantly correlated with the average nighttime depth ($r^2 = 0.32$, $p < 0.001$). On average, the nighttime depth was 13 m deeper than the lower thermocline margin (±2.5 m at 95% confidence interval). Only at one location was the *C. euxinus* layer 4.6 m above the 11 °C contour. However, the temperature was still below 15 °C; thus, the *C. euxinus* remained below the warm surface layer. A small portion of the scattering layer, possibly diapausing individuals, remained in the same depth both day and night.

Discussion

Although copepods can have an acoustic frequency response (FR) signature that can be used for their recognition, they are not easily detectable because they scatter sound weakly at frequencies commonly used in fisheries surveys. Furthermore, in many ecosystems, copepods occur in zooplankton communities of heterogeneous species composition, and their contribution to the overall measured backscattering can often be overwhelmed by that of more abundant, large, and/or strongly scattering organisms such as euphausiids, siphonophores, or pteropods (Lawson *et al.* 2004; Lavery *et al.* 2007). However, in this work, we present the unique case of the Black Sea, where the copepods form dense and well-isolated aggregations in low-oxygen layers at shallow depths. Multi-frequency acoustics was used to quantify the spatial distribution of the late developmental stages of the important planktonic prey *C. euxinus*. The late copepodite stages of this species are confined to depths <150 m due to anoxia. Their prosome length of over 2 mm, coupled with the low abundances of other scatterers, appeared to provide sufficiently strong returns for detection. In a study of *Neocalanus cristatus* and *Eucalanus bungii* copepods of length ca. 4.5 mm in the western North Pacific, Murase *et al.* (2009) assumed that at least 550–1445 individuals m^{-3} must be present to be detected at 38 kHz. We found that when sufficiently isolated in the water column at shallow depths, the minimum density of copepods required for detection could be as low as 157 individuals m^{-3}, as confirmed by our stratified net sampling. The ground truthed layers at the five stations provided a reference dataset for classification of the entire dataset using virtual echograms (shown in Figure 3). The pronounced acoustic FR evident in the observed data and confirmed with TS modelling enabled the classification to be robust, which is rare in the literature on copepods. Previous studies have used systems such as TAPS ("Tracor Acoustic Profiling System"; Holliday and Pieper, 1980), which is a high-frequency profiling system that samples a small volume at short range (typically 1 m) to quantify copepod abundance and spatial distribution. This and similar systems rely on a small sample volume, which mostly excludes larger scatterers, and on a short sample range, which minimizes the attenuation that occurs at high frequency with increasing range. However, to the best of our knowledge, the present work is the first to report the quantitative biomass distribution of a copepod species estimated acoustically over large spatial scales using a hull-mounted echo sounder operating at typical fisheries frequencies.

Our results provide confirmation of the general distribution characteristics of *C. euxinus* determined using net sampling by earlier studies (Svetlichny et al. 2006). In addition, our high-resolution acoustic sampling provides insight into the fine-scale structures that are associated with hydrographic features and reveals new aspects of copepod behaviour. In the Black Sea, the biochemical properties of the water column typically follow density contours (Tebo *et al.*, 1991, Tuğrul *et al.*, 1992). Consistent with this pattern, the daytime positioning of *C. euxinus* was more closely associated with water density than depth (Figure 7). The backscatter data demonstrated that almost the entire population remains in the OMZ during the daytime, between $\sigma_T = 15.2$ and 15.9 kg m^{-3}, generally shallower than 100 m. The diel vertical migration behaviour observed in this study is most likely undertaken to take refuge in the low oxygen zones (Hays, 2003). *C. euxinus* is known to have extensive oxygen tolerance (Vinogradov *et al.*, 1992). The vertical resolution in our measurements is sufficient to elucidate the depths of the dense concentrations and thereby the exact preference of this species in terms of its position with respect to depth or seawater density. The acoustic measurements also show for the first time that the majority of the population remains below the thermocline during the nighttime. The strong thermal stratification in summer may indirectly provide an advantage to the species as protection from the abundance of planktivorous small pelagic fish and gelatinous predators dominating the surface layer.

Our results indicate a patchy distribution, with a generally increasing trend in abundance from the inshore to the offshore and a pronounced peak at the continental slope. This patchiness is likely controlled by the circulation. Svetlichny *et al.* (2006) reported that the late copepodite stages of *C. euxinus* dominate the deep zones of the Black Sea, particularly the Rim current system, where the density of adults (female) varies from 1200 ind. m^{-2} to 2100 ind. m^{-2}. Our observations are consistent with these densities and spatial distribution, particularly with respect to the Rim current system (Figure 5; peak corresponds to this location). In addition, Svetlichny *et al.* (2006) reported an intense concentration of female individuals exceptionally close to shore near the central portion of the south coast, which was associated with gyres separating from the Rim current. This observation is also consistent with our results, and although our observations were localized further to the west, the dense zooplankton patches were potentially driven by similar mesoscale physical structures (Figure 1b). It is likely that these dense patches accumulate and are retained in the near-shore zone due to the quasi-permanent anticyclonic eddies that are generally observed in these areas (Ivanov *et al.*, 1998).

The consistency of the net and acoustic estimates of abundance allowed us to attempt to estimate the biomass. In addition to conventional methods, geostatistics were also used to estimate the total biomass due to the spatial autocorrelation in the data. The biomass calculated for the southern half of the Black Sea basin (Turkish EEZ) using ordinary kriging was 550 000 tons wet weight, 60 000 tons higher than that estimated with the conventional method. This difference was due to the high number of zero values at near-shore regions and few very dense patches constrained to small areas. This discrepancy can be further reduced by apportioning the data into sub-areas and taking the spatial structure into account (Maravelias *et al.*, 1996). To the best of our knowledge, this acoustically inferred biomass is the first estimated for the region.

Validation

The validation source used for this analysis was initially a dataset for ichthyoplankton collected with 500-μm mesh size plankton net. Although this net can effectively collect late copepodite stages of *C. euxinus* with body widths over 500 μm, it does not represent earlier developmental stages (<C4) and other small copepods. The un-sampled organisms smaller than the mesh size were not considered detectable with the acoustic frequency range used. Despite the potential underestimation of the overall composition, these net samples were suitable validation sources for the study purposes. Furthermore, the low estimation of earlier developmental stages is unlikely to cause a significant bias, as earlier studies confirm the numerical dominance of larger individuals during the summer, particularly within offshore populations (Yuneva *et al.*, 1999).

The comparison with net sampling produced encouraging correlations suggesting that spatial variability was successfully represented and the estimations are within the same order of magnitude as the net samples (Figure 9). It is also important to note that the chaetognath *Sagitta setosa* was also present in the nets. A difference in the backscattering potential is expected between *S. setosa* and *C. euxinus* due to their material properties of different dry weight to wet-weight ratios (*S. setosa*: ~0.08; *C. euxinus*: ~0.26; Arashkevich *et al.*, 2014). However, clear discrimination between chaetognaths and copepods proved difficult with the acoustic instruments employed. Although our assumption that the extracted signal is exclusively *C. euxinus* may not be entirely validated, the magnitude of the correlations with the net estimations shows that at least the main backscattering signal was dominated by *C. euxinus*. We assume that the contribution of chaetognaths to the backscatter can be neglected due to their high body water content; however, this assumption should be further tested by appropriate experiments.

Earlier acoustic studies focusing on the vertical position of zooplankton in the Black Sea also addressed this problem (Erkan and Gücü, 1999; Svetlichny *et al.*, 2000; Mutlu, 2003, 2006). Mutlu (2003) hypothesized that the acoustically detected swimming speed of *C. euxinus* within the OMZ could be used as an identification criterion for the concentration layers of the species and that this may help discriminate between *C. euxinus* and chaetognaths (Mutlu, 2006). However, he inferred the swimming speeds from independently analysed acoustical records of 120 and 200 kHz single-beam echo sounders, disregarding frequency responses. We believe that the upward swimming calculations might be biased for two reasons. First, the aggregations diffuse prior to the ascent, in contrast to the compact nighttime formation, thus adding significant subjectivity to the individual swimming speed estimation. Second, it is difficult to determine whether small changes in the depth of the *C. euxinus* layer result from upward swimming or variation in the depth of the OMZ, which varies considerably with the region. Nonetheless, the observed summertime acoustic patterns are consistent with our study, particularly the DVM onset, duration, and the interaction with the OMZ, although the previous study did not discern the association of the summertime acoustic patterns with the base of the thermocline.

Potential sources of uncertainty

The acoustic measurements may have several sources of uncertainty, both systematic and random. Sources of potential bias that are generally inherent in acoustic measures (Demer, 2004) include target classification, target strength estimation (model parameterization), spatial–temporal variations (in terms of size composition and length-to-weight conversion), signal processing, and survey area definition. The target strength model may be biased by values used for *g* and *h*. For example, the sensitivity analyses reported in the results, which were based on a range of *g* values reported in the literature, caused the estimates of biomass and abundance to vary by 45.6 and 75.4%, respectively. During dormancy, *Calanus* contain high amounts of lipids, which may alter *g*. DVM may also cause measurement bias. In this study, the nighttime backscatter was 27% lower than in the daytime

(Figure 8). Application of the TCF eliminated the day-night difference, but it also smoothed some of the spatial variation in the data (Figure 8). Particularly at higher frequencies, acoustic absorption may limit the maximum observation range. In this survey, however, the targets were shallow enough to allow high signal-to-noise detections at three frequencies, which facilitated target identification.

The Z-score method (De Robertis *et al.*, 2010) enabled classification by assuming, consistent with De Robertis *et al.* (2010), that the ΔS_v specific to *C. euxinus* was spatially consistent throughout the study area. This assumption may have been violated during the vertical migration phase, when animal orientations and thus acoustic incidence angles change. The average $\Delta S_{v,\ 120\text{–}38}$ determined for *C. euxinus* from the daytime concentration layers was 16.8 dB, which is a slightly lower value than the values calculated by Murase *et al.* (2009) for the copepod *Neocalanus cristatus* of average length of 4.3 mm in the western North Pacific (average $\Delta S_{v,120\text{–}38} = 17.3$ dB). The $\Delta S_{v,120\text{–}38}$ distribution was further corroborated by the DWBA model outputs, which produced reasonable agreement (19 dB for 120–38 kHz (Figures 4 and 8). However, $\Delta S_{V,\ 200\text{–}120}$ differed from the model by 3 dB, which begs further investigation.

Despite the background noise, the 200 kHz backscatter was useful, particularly during the nighttime, when *C. euxinus* was positioned near the surface. Here, the aggregation density was less intense than during the daytime, rendering the 38 kHz potentially susceptible to signal-to-noise ratio failure. However, 200 kHz improved the *Z*-scores; hence, classification was enhanced by additional detections (up to 46%) compared to the 120–38 kHz pair alone.

Considering the signal to noise ratio, the quality of the 120 kHz data tends to decrease with depth, with an apparently critical depth at 150 m. Consequently, the abundance estimation at the easternmost region of the study area, where the OMZ depth extends to below 150 m due to the anticyclonic gyre, is considered negatively biased (Figure 4). Furthermore, the aggregation pattern was more diffuse in this region, increasing the susceptibility to negative detection bias. Some brief trials showed that this range could be slightly improved by increasing the pulse duration to 1024 µs; however, this was not applied to maintain consistency during the course of the survey.

Conclusion

We estimated the distribution and abundance of the copepod *C. euxinus* based on multi-frequency acoustic data (38, 120, and 200 kHz). The backscattering characteristics of *C. euxinus* extracted from the daytime layers enabled acoustic classification. The abundance estimations of *C. euxinus* were consistent with the net counts. Our results also highlight the role of key physical properties: (1) the thermocline poses an upper barrier to the shallow nighttime phase of the diel vertical migration during summer and thereby protects *C. euxinus* from the potential warm water predators. (2) Highly dense patches of *C. euxinus* occur in the peripheral zones of the central gyres following the shelf edge, which may have important implications for fish distribution dynamics in the Black Sea. Acoustics provide precise information on the horizontal and vertical location of *C. euxinus* layers, which is important for both abundance estimates and ecological studies investigating the biogeochemical properties of these layers. The methods employed here are easily applied to data from similar surveys. Once established as a protocol, it is possible to monitor the population of this important copepod species and its interannual variability. Ecosystem modelling studies can greatly benefit from such information, which may eventually contribute to decision making in fisheries management.

Supplementary data

Supplementary material is available at the *ICESJMS* online version of the manuscript.

Acknowledgements

This study was conducted as part of a national anchovy fisheries project (KAMAG-110G124) funded by the Turkish Scientific and Technical Council, TUBITAK. We are thankful to Alexandra Gubanova for her contribution to plankton counts used in validation. We are grateful to Heather Cannaby for reviewing the manuscript and providing valuable comments and suggestions. We are grateful to Gareth Lawson for providing the MATLAB codes for the DWBA model and for his valuable insights and comments. We thank Melted Ok, Ezgi Şahin, Özge Tutar, and the crew of R/V Bilim2. We also thank Alison Kideys for her linguistic corrections on an earlier version of the manuscript. We are thankful to David Demer for his helpful and constructive editing suggestions. We thank two reviewers for their detailed comments and valuable suggestions. We also thank to Diana Ruiz Pino for her valuable comments in structuring the manuscript.

References

Arashkevich, E. G., Stefanova, K., Bandelj, V., Siokou, I., Kurt, T. T., Orek, Y. A., Timofte, F., et al. 2014. Mesozooplankton in the open Black Sea: regional and seasonal characteristics. Journal of Marine Systems, 135: 81–96.

Ballon, M., Bertrand, A., Lebourges-Dhaussy, A., Gutierrez, M., Ayon, P., Grados, D., and Gerlotto, F. 2011. Is there enough zooplankton to feed forage fish populations off Peru? An acoustic (positive) answer. Progress in Oceanography, 91: 360–381.

Besiktepe, S. 2001. Diel vertical distribution, and herbivory of copepods in the south-western part of the Black Sea. Journal of Marine Systems, 28: 281–301.

Besiktepe, S., Kideys, A. E., and Unsal, M. 1998. In situ grazing pressure and diet vertical migration of female *Calanus euxinus* in the Black Sea. Hydrobiologia, 363: 323–332.

Besiktepe, S., Svetlichny, L., Yuneva, T., Romanova, Z., and Shulman, G. 2005. Diurnal gut pigment rhythm and metabolic rate of *Calanus euxinus* in the Black Sea. Marine Biology, 146: 1189–1198.

De Robertis, A., and Higginbottom, I. 2007. A post-processing technique to estimate the signal-to-noise ratio and remove echosounder background noise. ICES Journal of Marine Science, 64: 1282–1291.

De Robertis, A., McKelvey, D. R., and Ressler, P. H. 2010. Development and application of an empirical multifrequency method for backscatter classification. Canadian Journal of Fisheries and Aquatic Sciences, 67: 1459–1474.

Demer, D. A., and Hewitt, R. P. 1995. Bias in acoustic biomass estimates of Euphausia-Superba due to diel vertical migration. Deep-Sea Research Part I-Oceanographic Research Papers, 42: 455–475.

Demer, D. A., and Conti, S. G. 2003. Reconciling theoretical versus empirical target strengths of krill: effects of phase variability on the distorted-wave Born approximation. ICES Journal of Marine Science: Journal Du Conseil, 60: 429–434.

Demer, D. A. 2004. An estimate of error for the CCAMLR 2000 survey estimate of krill biomass. Deep Sea Research Part II: Topical Studies in Oceanography, 51: 1237–1251.

Erkan, F., and Gucu, A. C. 1999. Analyzing ship-borne acoustic Doppler current profiler measurements to estimate the vertical and spatial distribution of southern Black Sea zooplankton. The Journal of the Acoustical Society of America, 105: 1050.

Foote, K. G., Knudsen, H. P., Vestnes, G., MacLennan, D. N., and Simmonds, E. J. 1987. Calibration of acoustic instruments for fish density estimation: a practical guide. ICES Cooperative Research Report 144: 81.

Foote, K., and Stanton, T. 2000. Acoustical methods. ICES Zooplankton Methodology Manual, 223–258.

Gücü, A. C., Inanmaz, ÖE., Ok, M., and Sakinan, S. 2016. Recent changes in the spawning grounds of Black Sea anchovy, *Engraulis encrasicolus*. Fisheries Oceanography, 25: 67–84.

Hays, G. C. 2003. A review of the adaptive significance and ecosystem consequences of zooplankton diel vertical migrations. Hydrobiologia, 503: 163–170.

Holliday, D. V., and Pieper, R. E. 1980. Volume scattering strengths and zooplankton distributions at acoustic frequencies between 0.5 and 3 MHz. The Journal of the Acoustical Society of America, 67: 135–146.

Holliday, D. V., Pieper, R. E., and Kleppel, G. S. 1989. Determination of zooplankton size and distribution with multifrequency acoustic technology. Journal Du Conseil, 46: 52–61.

Ivanov, L. I., and Oguz, T. and North Atlantic Treaty Organization. Scientific Affairs Division. 1998. Ecosystem Modeling as a Management Tool for the Black Sea. Kluwer Academic Publishers, Dordrecht, Boston.

Korneliussen, R. J., Diner, N., Ona, E., Berger, L., and Fernandes, P. G. 2008. Proposals for the collection of multifrequency acoustic data. ICES Journal of Marine Science, 65: 982–994.

Lavery, A. C., Wiebe, P. H., Stanton, T. K., Lawson, G. L., Benfield, M. C., and Copley, N. 2007. Determining dominant scatterers of sound in mixed zooplankton populations. Journal of the Acoustical Society of America, 122: 3304–3326.

Lawson, G. L., Wiebe, P. H., Ashjian, C. J., Gallager, S. M., Davis, C. S., and Warren, J. D. 2004. Acoustically-inferred zooplankton distribution in relation to hydrography west of the Antarctic Peninsula. Deep Sea Research Part II: Topical Studies in Oceanography, 51: 2041–2072.

Lezama-Ochoa, A., Ballon, M., Woillez, M., Grados, D., Irigoien, X., and Bertrand, A. 2011. Spatial patterns and scale-dependent relationships between macrozooplankton and fish in the Bay of Biscay: an acoustic study. Marine Ecology Progress Series, 439: 151–168.

Maravelias, C. D., Reid, D. G., Simmonds, E. J., and Haralabous, J. 1996. Spatial analysis and mapping of acoustic survey data in the presence of high local variability: geostatistical application to North Sea herring (*Clupea harengus*). Canadian Journal of Fisheries and Aquatic Sciences, 53: 1497–1505.

McKelvey, D. R., and Wilson, C. D. 2006. Discriminant classification of fish and zooplankton backscattering at 38 and 120 kHz. Transactions of the American Fisheries Society, 135: 488–499.

Mitson, R. B., Simard, Y., and Goss, C. 1996. Use of a two-frequency algorithm to determine size and abundance of plankton in three widely spaced locations. ICES Journal of Marine Science, 53: 209–215.

Murase, H., Ichihara, M., Yasuma, H., Watanabe, H., Yonezaki, S., Nagashima, H., Kawahara, S., et al. 2009. Acoustic characterization of biological backscatterings in the Kuroshio-Oyashio interfrontal zone and subarctic waters of the western North Pacific in spring. Fisheries Oceanography, 18: 386–401.

Mutlu, E. 2003. Acoustical identification of the concentration layer of a copepod species, *Calanus euxinus*. Marine Biology, 142: 517–523.

Mutlu, E. 2005. A comparison of the contribution of zooplankton and nekton taxa to the near-surface acoustic structure of three Turkish seas. Marine Ecology: An Evolutionary Perspective, 26: 17–32.

Mutlu, E. 2006. Diel vertical migration of Sagitta setosa as inferred acoustically in the Black Sea. Marine Biology, 149: 573–584.

Mutlu, E. 2007. Acoustical scattering layers of two mesozooplanktons as a tool for hydrographic features of the Black Sea. Journal of Applied Biological Sciences, 1: 01–08.

Murray, J. W., Stewart, K., Kassakian, S., Krynytzky, M., and DiJulio, D. 2006. Oxic, suboxic and anoxic conditions in the Black Sea. *In* Climate Change and Coastline Migration as Factors in Human Adaptation to the Circum-Pontic Region: From Past to Forecast. A., Gilbert, V., YankoHombach, and N., Panin, Eds. Kluwer, New York. pp. 437–452.

Omori, M., and Hamner, W. M. 1982. Patchy distribution of zooplankton—behavior, population assessment and sampling problems. Marine Biology, 72: 193–200.

Ressler, P. H., De Robertis, A., Warren, J. D., Smith, J. N., and Kotwicki, S. 2012. Developing an acoustic survey of euphausiids to understand trophic interactions in the Bering Sea ecosystem. Deep-Sea Research Part II-Topical Studies in Oceanography, 65–70: 184–195.

Simmonds, J., and MacLennan, D. N. 2005. Fisheries Acoustics: Theory and Practice, 2nd edn. Blackwell Science, Oxford, UK. 437 pp.

Staneva, J. V., Dietrich, D. E., Stanev, E. V., and Bowman, M. J. 2001. Rim current and coastal eddy mechanisms in an eddy-resolving Black Sea general circulation model. Journal of Marine Systems, 31: 137–157.

Stanton, T. K., and Chu, D. Z. 2000. Review and recommendations for the modelling of acoustic scattering by fluid-like elongated zooplankton: euphausiids and copepods. ICES Journal of Marine Science, 57: 793–807.

Stanton, T. K., Chu, D. Z., and Wiebe, P. H. 1996. Acoustic scattering characteristics of several zooplankton groups. ICES Journal of Marine Science, 53: 289–295.

Stepnowski, A., Gücü, A. C., and Bingel, F. 1993. Assessment of the pelagic fish resources in the southern Black Sea using echo integration and dual-beam processing. Archives of Acoustic, Polish Academy of Science Journal, 18: 83–104.

Svetlichny, L. S., and Hubareva, E. S. 2005. The energetics of *Calanus euxinus*: locomotion, filtration of food and specific dynamic action. Journal of Plankton Research, 27: 671–682.

Svetlichny, L. S., Hubareva, E. S., Erkan, F., and Gucu, A. C. 2000. Physiological and behavioral aspects of *Calanus euxinus* females (Copepoda: Calanoida) during vertical migration across temperature and oxygen gradients. Marine Biology, 137: 963–971.

Svetlichny, L. S., Kideys, A. E., Hubareva, E. S., Besiktepe, S., and Isinibilir, M. 2006. Development and lipid storage in *Calanus euxinus* from the Black and Marmara seas: variabilities due to habitat conditions. Journal of Marine Systems, 59: 52–62.

Svetlichny, L. S., Yuneva, T. V., Hubareva, E. S., Schepkina, A. M., Besiktepe, S., Kideys, A. E., Bat, L., et al. 2009. Development of *Calanus euxinus* during spring cold homothermy in the Black Sea. Marine Ecology Progress Series, 374: 199–213.

Tebo, B. M., Rosson, R. A., and Nealson, K. H. 1991. Potential for manganese (II) oxidation and manganese (IV) reduction to cooccur in the suboxic zone of the Black Sea. *In* Black Sea Oceanography (pp. 173–185), Izder, E., Murray, J. W., Eds. Springer, Netherlands.

Tuzhilkin, V. S. 2008. Thermohaline structure of the sea. *In* The Black Sea Environment: The Handbook of Environmental Chemistry, Vol. 5, part Q, pp. 217–253, A. G., Kostianoy, A. N., Kosarev, Eds. Springer, Berlin.

Thorisson, K. 2006. How are the vertical migrations of copepods controlled? Journal of Experimental Marine Biology and Ecology, 329: 86–100.

Tuğrul, S., Basturk, O., Saydam, C., and Yılmaz, A. 1992. Changes in the hydrochemistry of the Black-Sea inferred from water density profiles. Nature, 359: 137–139.

Vinogradov, M. E., Arashkevich, E. G., and Ilchenko, S. V. 1992. The ecology of the *Calanus*-Ponticus population in the deeper layer of its concentration in the Black-Sea. Journal of Plankton Research, 14: 447–458.

Vinogradov, M. E., Flint, M. V., and Shushkina, E. A. 1985. Vertical-distribution of mesoplankton in the open area of the Black-Sea. Marine Biology, 89: 95–107.

Wiebe, P. H., and Benfield, M. C. 2003. From the Hensen net toward four-dimensional biological oceanography. Progress in Oceanography, 56: 7–136.

Yuneva, T. V., Svetlichny, L. S., Yunev, O. A., Romanova, Z. A., Kideys, A. E., Bingel, F., Uysal, Z., et al. 1999. Nutritional condition of female *Calanus euxinus* from cyclonic and anticyclonic regions of the Black Sea. Marine Ecology Progress Series, 189: 195–204.

Handling editor: David Demer